Aerosol–cloud drop concentration closure in warm cumulus

W. C. Conant,[1] T. M. VanReken,[2] T. A. Rissman,[2] V. Varutbangkul,[2] H. H. Jonsson,[3] A. Nenes,[4] J. L. Jimenez,[5] A. E. Delia,[6] R. Bahreini,[1] G. C. Roberts,[7] R. C. Flagan,[1,2] and J. H. Seinfeld[1,2]

Received 3 November 2003; revised 29 April 2004; accepted 14 May 2004; published 14 July 2004.

[1] Our understanding of the activation of aerosol particles into cloud drops during the formation of warm cumulus clouds presently has a limited observational foundation. Detailed observations of aerosol size and composition, cloud microphysics and dynamics, and atmospheric thermodynamic state were collected in a systematic study of 21 cumulus clouds by the Center for Interdisciplinary Remotely-Piloted Aircraft Studies (CIRPAS) Twin Otter aircraft during NASA's Cirrus Regional Study of Tropical Anvils and Cirrus Layers–Florida Area Cirrus Experiment (CRYSTAL-FACE). An "aerosol-cloud" closure study was carried out in which a detailed cloud activation parcel model, which predicts cloud drop concentration using observed aerosol concentration, size distribution, cloud updraft velocity, and thermodynamic state, is evaluated against observations. On average, measured droplet concentration in adiabatic cloud regions is within 15% of the predictions. This agreement is corroborated by independent measurements of aerosol activation carried out by two cloud condensation nucleus (CCN) counters on the aircraft. Variations in aerosol concentration, which ranged from 300 to 3300 cm^{-3}, drives large microphysical differences (250–2300 cm^{-3}) observed among continental and maritime clouds in the South Florida region. This is the first known study in which a cloud parcel model is evaluated in a closure study using a constraining set of data collected from a single platform. Likewise, this is the first known study in which relationships among aerosol size distribution, CCN spectrum, and cloud droplet concentration are all found to be consistent with theory within experimental uncertainties much less than 50%. Vertical profiles of cloud microphysical properties (effective radius, droplet concentration, dispersion) clearly demonstrate the boundary layer aerosol's effect on cloud microphysics throughout the lowest 1 km of cloud depth. Onboard measurements of aerosol hygroscopic growth and the organic to sulfate mass ratio are related to CCN properties. These chemical data are used to quantify the range of uncertainty associated with the simplified treatment of aerosol composition assumed in the closure study. *INDEX TERMS:* 0305 Atmospheric Composition and Structure: Aerosols and particles (0345, 4801); 0320 Atmospheric Composition and Structure: Cloud physics and chemistry; 0345 Atmospheric Composition and Structure: Pollution—urban and regional (0305); 1610 Global Change: Atmosphere (0315, 0325); 3314 Meteorology and Atmospheric Dynamics: Convective processes; *KEYWORDS:* aerosol, CCN, cloud microphysics

Citation: Conant, W. C., et al. (2004), Aerosol–cloud drop concentration closure in warm cumulus, *J. Geophys. Res.*, *109*, D13204, doi:10.1029/2003JD004324.

1. Introduction

[2] Satellite and aircraft observations have corroborated predictions that particulate pollution increases cloud albedo and decreases precipitation efficiency [*Twomey*, 1977; *Albrecht*, 1989; *Rosenfeld and Lensky*, 1998; *Ackerman et al.*, 2000]. Because such effects alter Earth's climate by perturbing the radiation balance and hydrological cycle, they are called indirect effects of aerosol on climate, or

[1]Department of Environmental Science and Engineering, California Institute of Technology, Pasadena, California, USA.
[2]Department of Chemical Engineering, California Institute of Technology, Pasadena, California, USA.
[3]Center for Interdisciplinary Remotely-Piloted Aircraft Studies, Naval Postgraduate School, Monterey, California, USA.
[4]Schools of Earth and Atmospheric Sciences and Chemical and Biomolecular Engineering, Georgia Institute of Technology, Atlanta, Georgia, USA.
[5]Department of Chemistry and Biochemistry, Cooperative Institute for Research in Environmental Sciences, University of Colorado, Boulder, Colorado, USA.
[6]Program in Atmospheric and Oceanic Sciences, University of Colorado, Boulder, Colorado, USA.
[7]Center for Atmospheric Sciences, Scripps Institution of Oceanography, University of California, San Diego, La Jolla, California, USA.

0148-0227/04/2003JD004324

simply "indirect effects" [*Houghton et al.*, 2001]. To have confidence in predictions of indirect effects, it is necessary to develop physically based and observationally validated models of the sensitivity of cloud microphysics to the properties of the cloud condensation nuclei (CCN) on which the cloud forms. The most fundamental of these models is the adiabatic parcel model, which predicts cloud drop concentrations within ascending air parcels by simulating the transfer of water vapor and heat between the adiabatically cooling parcel and the CCN within using a first principles treatment of chemical and thermodynamic processes. These models are used as tools to formulate and validate the relatively simpler parameterizations that are used in cloud-resolving models and global climate simulations [e.g., *Nenes and Seinfeld*, 2003].

[3] In an attempt to give such models a firm observational foundation, two closure studies were conducted during NASA's Cirrus Regional Study of Tropical Anvils and Cirrus Layers–Florida Area Cirrus Experiment (CRYSTAL-FACE). The first of these studies [*VanReken et al.*, 2003] finds that measured CCN concentrations at 0.2% and 0.85% supersaturations agree to within 10–20% of that predicted by Köhler theory given measured aerosol concentration and size distribution. This is termed aerosol-CCN closure. If chemical and kinetic effects on cloud activation are relatively minor, one could proceed to predict cloud drop number concentration (CDNC) directly from the measured CCN spectrum and observed updraft velocity in a CCN-CDNC closure [e.g., *Snider and Brenguier*, 2000]. Studies that attempt CCN-CDNC closure have generally been successful within a factor of ~50% [*Twomey and Warner*, 1967; *Fitzgerald and Spyers-Duran*, 1973; *Snider and Brenguier*, 2000]. In contrast, aerosol-CCN closure attempts have met with more limited success, such that predicted CCN often exceeds measured values (see review by *Chuang et al.* [2000]). The lack of aerosol-CCN closure brings into question either (1) our fundamental understanding of the role of aerosol composition on the CCN spectrum ("chemical effects," see *Nenes et al.* [2002]) or (2) the techniques used to determine CCN spectrum or composition and mixing state. If CCN instrument bias is the source of the problem, however, this has implications for previous studies that found CCN-CDNC closure. A different strategy is taken here, in which a cloud model that predicts cloud drop concentration directly from updraft velocity and the aerosol physicochemical properties is evaluated against observations. This is termed aerosol-CDNC closure, in which the computation of CCN spectrum as an intermediary step is implicit. Taken together, aerosol-CCN closure and aerosol-CDNC closure provide a rigorous test on our understanding of how aerosol controls cloud microphysics.

[4] CRYSTAL-FACE was conducted during July 2002 from Boca Chica Naval Air Station near Key West, Florida (Figure 1). The Center for Interdisciplinary Remotely-Piloted Aircraft Studies (CIRPAS) Twin Otter, one of six aircraft deployed during CRYSTAL-FACE, provided redundant and calibrated measurements of aerosol concentration and size distribution from 0.003 to 5 μm; mass concentrations of sulfate, organic carbon, nitrate, and ammonium from 0.1 to 0.6 μm; cloud condensation nucleus (CCN) concentration at 0.2% and 0.85% supersaturation; cloud drop concentration and size distribution from 1 to 1600 μm;

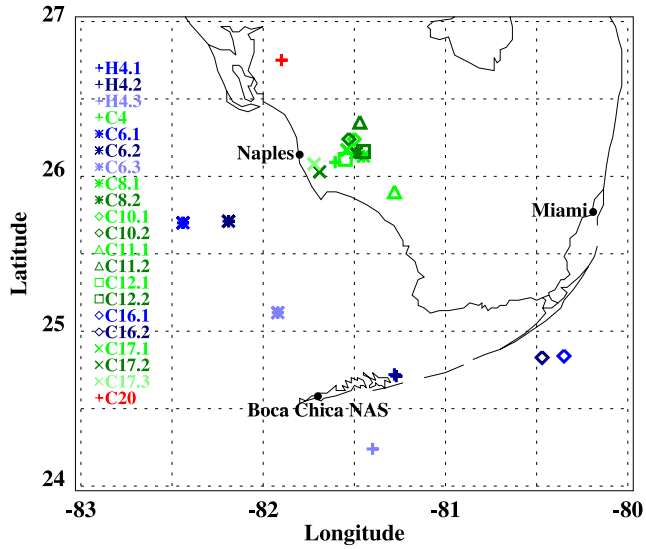

Figure 1. Map of the CRYSTAL-FACE region in South Florida. Each symbol denotes the location of a cloud characterized by the Twin Otter.

and absolute wind speed with 0.35 m s^{-1} accuracy, which is derived from a gust probe on the nose of the aircraft and internal navigation and GPS positioning systems following *Lenschow* [1986] (Table 1). Cumulus clouds were characterized by flying several successively higher constant altitude legs, starting with one or two legs below cloud base to obtain the aerosol properties and thermodynamic state of the air entrained through cloud base; the final legs often ended more than 2500 m above cloud base. Nine flights were dedicated to this strategy, during which 20 clouds were profiled (Table 2). These flights were conducted over land and ocean with concentrations of CCN(0.85%) ranging from 300 cm^{-3} to 3300 cm^{-3} and cloud core drop concentrations ranging from 250 cm^{-3} to 2300 cm^{-3}. These data provide a wide range of conditions necessary to evaluate models of aerosol effects on warm cumulus microphysics.

2. Aerosol-CDNC Closure

[5] The *Nenes et al.* [2002] model simulates the activation of aerosol into cloud drops by numerically integrating the equations describing the rate of transfer of heat and water vapor between the gas and particulate phases for a parcel rising at constant updraft velocity [e.g., *Pruppacher and Klett*, 1997]. Initial temperature, pressure, humidity, and updraft velocity are specified along with a sufficient number of lognormal modes required to describe the dry aerosol size distribution (4 modes are used here, divided into 50 size bins per mode). Dry aerosol composition (NH_4^+, SO_4^{2-}, Na^+ Cl^-) and insoluble aerosol fraction are specified separately for each mode. It is known that soluble gases (e.g., HNO_3) and various organic species may have chemical effects (i.e., partial solubility, surface activity, film-forming tendency) that influence the CCN spectrum and the cloud activation process [*Nenes et al.*, 2002]. Although the model is designed to simulate such chemical effects, they are assumed negligible here. This model compares well with other explicit cloud activation models when standard cases are used as input [*Kreidenweis et al.*, 2003]. The conden-

Table 1. Aerosol, Cloud, and Meteorological Instrumentation for the Office of Naval Research CIRPAS Twin Otter Aircraft During CRYSTAL-FACE

Measurement	Instrument	Measurement Parameters	Measurement Principle
Aerosol concentration	condensation particle counters (3)	geometric diameter > {3 nm, 7 nm, 13 nm}	varying supersaturations of butanol
Aerosol size distribution	Dual Autostatic Classifier Detector System (DACADS)	geometric diameter: 15–800 nm	electrostatic classification; dry and ambient humidity
	Aerosol Spectrometer Probe (PCASP)	geometric diameter: 100–2500 nm	optical scattering
	Aerodynamic Paricle Sizer (APS)	aerodynamic diameter: 500–10,000 nm	aerodynamic classification
Cloud and aerosol size distribution	Forward Scattering Spectrometer Probe (FSSP)	geometric diameter: 3–47 μm	optical forward scattering
	Cloud and Aerosol Particle Spectrometer (CAPS)	geometric diameter: 0.5–1600 μm	optical forward scattering and two-dimensional imaging
CCN concentration	Caltech CCN counter	$S_C < 0.85\%$	continuous flow; increasing temperature
	Scripps CCN counter	$S_C < 0.2\%$	continuous flow; increasing temperature
Aerosol composition	Aerodyne Aerosol Mass Spectrometer (AMS)	mass concentration: SO_4^{2-}, NH_4^+, NO_3^-, OC 100–600 nm	flash ionization; quadrapole mass spectrometer
Updraft velocity and wind speed	five-hole turbulence probe, C-MIGITS inertial navigation system, and Novatel GPS	wind velocity; aircraft position and attitude	wind velocity = aircraft ground velocity (C-MIGITS INS/GPS) – aircraft air velocity (turbulence and Pitot-static probes)

sation coefficient for this study is taken to be 0.06 on the basis of the laboratory studies of *Shaw and Lamb* [1999]. (Other laboratory studies have found values ranging from 0.03 to 0.3; the standard value assumed in most cloud models is 0.042 [*Pruppacher and Klett*, 1997].) Particle surface tension is taken to be that of liquid water. Simulations are made for each cloud profiled during CRYSTAL FACE using aerosol properties and thermodynamic state measured beneath the cloud.

[6] Aerosol observations used as input to the model are obtained separately for each cloud in the following manner. Dry aerosol size measured by the Dual Autostatic Classifier Detector System (DACADS) (10–800 nm) and the Aerosol Spectrometer Probe (PCASP) optical probe (100–2500 nm) in the subcloud legs are merged into a single size distribution, averaged, and parameterized in the form of four lognormal modes. Submicrometer modes are taken to be ammonium bisulfate, which is consistent with the observed Aerodyne Aerosol Mass Spectrometer (AMS) NH_4^+:SO_4^{2-} ratios. Supermicrometer modes are presumed to be NaCl. Over land, the AMS composition (100–600 nm) often showed significant organic carbon (OC) content. OC is generally less soluble than sulfate aerosol [e.g., *Prenni et al.*, 2003; *Gysel et al.*, 2004] and may reduce aerosol surface tension [*Facchini et al.*, 1999]. These have opposite effects on the CCN spectrum, relative to sulfate aerosol. The impact of the reduced solubility on the CCN spectrum is smaller when the OC is internally mixed with sulfate. Because no comprehensive model for OC activation behavior yet exists, previous attempts at CCN prediction have typically implemented one of two assumptions: either OC is entirely insoluble and internally mixed

Table 2. Summary of Cloud Observations

Flight Number –Cloud Number	Date	Number of Passes (Below/In)	CCN 0.85%, cm^{-3}	σ CCN, cm^{-3}	N_A, cm^{-3} (35–800 nm)	OC/SO_4 Mass Ratio (100–600 nm)	w, m s^{-1}	N_D Predicted, cm^{-3}	N_D Observed, cm^{-3} Method 1	N_D Observed, cm^{-3} Method 2
H4-1	27 June	2/4	764	53	811	0.16	1.4	626	769	820
H4-2	27 June	2/3	1062	97	1049	0.15	1.0	699	959	1177
H4-3	27 June	2/11	515	17	510	0.13	0.9	382	413	409
C4	7 July	3/6	860	129	1025	0.4	2.2	830	1042	1427
C6-1	10 July	1/6	343	20	294	0.3	0.9	220	216	275
C6-2	10 July	2/11	407	156	309	0.3	1.8	279	280	272
C6-3	10 July	1/7	569	103	612	0.3	1.0	400	434	392
C8-1	13 July	1/6	NA[a]	NA	1167	1.3	1.5	847	1078	1277
C8-2	13 July	1/5	NA	NA	1034	1.5	1.9	938	936	935
C10-1	18 July	1/5	2785	124	3394	2.4	1.5	2239	2285	2279
C10-2	18 July	1/5	2783	111	3350	2.5	1.2	1893	1995	2167
C11-1	18 July	1/7	1746	40	1879	1.9	2.8	1666	1717	1959
C11-2	18 July	2/5	2520	210	3007	2.5	2.4	2358	2526	2667
C12-1	19 July	1/12	561	65	478	NA	2.4	469	523	575
C12-2	19 July	2/8	450	215	410	NA	2.2	397	633	641
C16-1	25 July	1/5	316	18	348	0.6	1.1	273	360	390
C16-2	25 July	1/3	316	18	348	0.5	1.6	312	330	426
C17-1	26 July	2/6	454	43	455	0.4	1.7	384	423	419
C17-2	26 July	1/7	305	30	373	0.3	1.6	306	493	363
C17-3	26 July	1/9	NA	NA	681	0.3	2.4	614	NA	642
C20[b]	29 July	1/1	967	387	1797	1.0	2.8	1225	1167	1167

[a]NA, not applicable.
[b]This was a brief pass into the base of a larger convective system.

with sulfate [e.g., *Snider and Brenguier*, 2000] or OC is treated as equivalent to ammonium sulfate (which rapidly approaches the insoluble and internally mixed assumption in the limit of low OC fraction) [e.g., *Rivera-Carpio et al.*, 1996]. *VanReken et al.* [2003] show that the aerosol-CCN closure at 0.2% and 0.85% in CRYSTAL-FACE was accurate to within 10–20% given an ammonium sulfate assumption, in spite of wide variability in the observed AMS OC:SO_4^{2-} ratio. Given this good agreement, we initially implement the simpler assumption that OC behaves like sulfate aerosol for the purposes of cloud activation. The appropriateness of this assumption will be examined in detail in section 4. In section 5, we study the implications of varying composition through a series of sensitivity studies. Concentration measured by the DACADS is tested against that measured by a TSI 3010 condensation particle counter (CPC), which measures all aerosol particles greater than 12 nm. In clear-air cases with stable CPC concentrations (standard deviation over 100 s < 15% of the mean), the DACADS and CPC concentrations agree with a negligible mean bias and a root-mean-square deviation of 20%. The DACADS-CPC difference is not sensitive to total concentration or mean aerosol size, indicating that no significant saturation or size-dependent biases exist for the range of conditions observed here. The inlet system for the Twin Otter cabin instruments was tested in a wind tunnel experiment, in which the transmission of particles from 10 to 2500 nm was indistinguishable from unity.

[7] The measured CCN spectrum is not taken as an input to the parcel model (see methods employed by *Twomey* [1959], *Snider and Brenguier* [2000], and *Snider et al.* [2003] for examples). Instead, full Köhler theory is employed at each stage of droplet growth, using the measured aerosol properties described above. *VanReken et al.* [2003] show 10–20% agreement between calculated and measured CCN concentrations at 0.2% and 0.85% during CRYSTAL-FACE assuming the aerosol composition is ammonium sulfate, which is similar to the assumption used here of ammonium bisulfate and sodium chloride. Thus the CCN spectrum implicitly assumed here when solving the droplet growth equations is consistent with the CCN observations. Certain chemical effects on droplet activation, such as those of surface-forming organic films [*Feingold and Chuang*, 2002] and water-soluble gases [*Laaksonen et al.*, 1998], are not strictly tested in aerosol-CCN closure. These effects can contribute to a lack of aerosol-CDNC closure, even in the event that there is good aerosol-CCN closure.

[8] Observations of updraft velocity were taken from below-cloud and cloud base legs. For the remainder of this paper, "cloud base" refers to the lowest 100 m of these cumulus clouds, which extended several kilometers in height and contained coherent updrafts hundreds of meters in horizontal extent. Updraft velocity is obtained from a combination of instruments, including a five-hole gust probe on the nose of the aircraft, a Pitot-static pressure tube, a Coarse/Acquistion Code–Micro-Electro-Mechanical Systems (MEMS) Integrated GPS/INS Tactical System (C-MIGITS) GPS/inertial navigation system (INS), and the Novatel GPS system. Calibrations for all wind variables are derived using the procedures outlined by *Lenschow* [1986]. The aircraft velocity estimated by the C-MIGITS system was reprocessed using position data from the more accurate Novatel GPS, while retaining the short-period response characteristics of the C-MIGITS INS, which is based on quartz accelerometers. Uncertainties in total air speed, INS-retrieved heading and pitch angles, GPS-retrieved aircraft velocity, and the accuracy of the gust probe differential pressure measurements combine for a total uncertainty in updraft velocity of 0.35 m s^{-1}. A number of model calculations are made for each cloud to obtain predicted CDNC(w) as a function of updraft velocity w. Then, a representative average CDNC(predicted) is obtained from

$$\mathrm{CDNC(predicted)} = \int \mathrm{CDNC}(w) w n(w) \mathrm{d}w \Big/ \int w n(w) \mathrm{d}w,$$

where $n(w)$ is the observed distribution of updraft velocity below and within cloud base and the w weighting is introduced to account for the higher mass flux across cloud base associated with stronger updrafts. This procedure produces CDNC predictions on average 0.5% lower than simply using mass-flux-weighted mean w.

[9] Droplet concentrations were observed at 1-Hz (~50 m) resolution using the Cloud and Aerosol Spectrometer (CAS) optical probe on board the Cloud, Aerosol, and Precipitation Spectrometer (CAPS) integrated spectrometer system [*Baumgardner et al.*, 2001]. The CAS measures droplet size from 0.5 to 60 μm in 20 size bins using a forward scattering principle similar to that of the Forward Scattering Spectrometer Probe (FSSP-100). Relative to the FSSP-100, the CAS contains certain design improvements that have (1) obviated the need for dead-time corrections at concentrations less than 26,000 cm^{-3} (at the Twin Otter air speed of 50 m s^{-1}) because of improved electronics, (2) reduced the frequency of coincidence errors by reducing the viewing volume and refining detection techniques, and (3) allowed for spectra to be obtained at lower sizes and finer size resolution by increasing laser power. These improvements make the CAS ideal for studying cloud activation, which requires observations to be close to cloud base, where droplets are still small and have activated sufficiently recently to dramatically improve the probability of finding nearly adiabatic conditions. Coincidence errors, which are typical of single-particle optical probes [e.g., *Baumgardner et al.*, 1985; *Burnet and Brenguier*, 2002], are estimated to decrease cloud drop concentrations by 1% at 800 cm^{-3} and 10% at 7000 cm^{-3}. Corrections to CDNC are applied using the principles outlined by *Burnet and Brenguier* [2002] and the CAS instrument characteristics (viewing area equals 0.112 mm^2; beam width equals 0.1 mm). Because of an improved CAS detection algorithm, particles outside the depth of field (DOF) do not contribute to coincidence errors in concentration as much as in the FSSP probes (D. Baumgardner, personal communication, 2004). The CAS size measurement was calibrated before, during, and after the campaign using monodisperse polystyrene and glass beads. Viewing volume is estimated to be accurate within 15% using geometric characterization of the CAS viewing area and typical uncertainties in flow rates [e.g., *Dye and Baumgardner*, 1984]. The particular CAS flown on the Twin Otter has shown stable properties in calibration and performance over its lifetime. Observed liquid water content (LWC) is measured by integrating the CAS size distribution.

The large cumulus cloud (H4.3) sampled on 27 June provides an opportunity to test the LWC measured by the CAS probe. The core of this cloud exhibited an adiabatic profile in equivalent potential temperature θ_e and LWC for each pass from 500 m (base) to 1700 m, meaning that at the core of the cloud, θ_e was constant to within 10% of the subcloud minus out-of-cloud θ_e difference and LWC was within 10% of the adiabatic calculation. Coincidence-related sizing errors [*Burnet and Brenguier*, 2002] are estimated to cause a range of uncertainty in LWC from −0.5% to +1% for this cloud, whose core contained droplet concentrations of 410 cm^{-3}. Coincidence uncertainties in LWC assume that coincidence events can be caused by particles within the viewing volume outside the DOF, which is assumed to have an effective sampling volume equal to that within the DOF [*Dye and Baumgardner*, 1984; D. Baumgardner, personal communication, 2004]. (Although the viewing volume outside the DOF is 2–3 times that within the DOF, the signals from particles outside the DOF are significantly reduced, thus limiting their contribution to coincidence artifacts on droplet size.) Uncertainties in determining the adiabatic LWC profile are small when compared with literature uncertainty estimates [e.g., *Lawson and Blyth*, 1998], because cloud base itself was determined within 30 m through cloud base penetrations. This determination was made microphysically, by observing GPS altitudes at the point where a cloud drop mode emerged from the haze in the observed CAS size distribution (0.5–50-μm diameter). On the basis of this accuracy in cloud base altitude the uncertainty in adiabatic LWC is better than 10% when more than 300 m above cloud base. Because this cloud consistently exhibited core LWC values within 10% of adiabatic calculations on each pass up to 1200 m above cloud base, a 15% uncertainty in CAPS LWC is taken. This can be used to evaluate uncertainties in mean droplet volume (nominal uncertainty 33%) and number concentration (nominal uncertainty 15%), the product of which is LWC. Assuming that uncertainty estimates above are uncorrelated and normally distributed, the 15% accuracy in LWC confirms the uncertainty estimate in number concentration of 15% and increases confidence in the sizing uncertainty estimate to within 18% for mean droplet volume and 6% for volumetric average diameter.

[10] Data for the model-observation comparison in cloud drop concentration are carefully screened to avoid the influences of entrainment mixing, which is not treated in the model simulations. First, droplets below 1-μm diameter are neglected as unactivated haze. (Alternative methods to define haze based on the minimum between the haze mode and the droplet mode produced equivalent results in determining droplet concentration.) Cloud drop concentration observations are selected on the basis of the following criteria: (1) The cloud drop effective diameter is greater than 2.4 μm ($d_e = \langle d^3\rangle/\langle d^2\rangle$, where $\langle\rangle$ indicates an average over the size distribution >1 μm); (2) it is narrow, having geometric standard deviation, $\sigma < 1.5$; (3), it contains no droplets larger than 30-μm diameter (to eliminate precipitation); and (4) cloud edge observations are neglected (i.e., both the preceding and subsequent observations must satisfy criteria 1–3). Furthermore, only the lowest passes through the cloud are taken, which were most often within 50 m of cloud base. Two methods are used to determine mean "cloud base droplet concentration" from the remaining data. For method 1, droplet concentration is averaged over those observations having LWC exceeding the mean adiabatic value. A range of adiabatic LWC values is determined separately for each cloud based on variability in lifting condensation level computed from subcloud measurements of pressure, water vapor mixing ratio q_g, and potential temperature θ and by assuming a moist adiabatic ascent through the cloud. Bias errors in lifting condensation level due to biases in the thermodynamic measurements are reduced through the microphysical determination of cloud base altitude discussed above. The average is obtained by weighting with updraft velocity (positive values only) to represent the mass flux through cloud base. The screening criterion that LWC exceed the mean adiabatic value minimizes the potential for including cloud regions strongly affected by entrainment, which tends to reduce droplet concentration and LWC. Method 2 screening is based on the observation that CDNC often contributes a much larger source of variability than volumetric mean diameter $\langle d^3\rangle$ to LWC (in these regions near cloud base). This is characteristic of artifacts related to averaging over cloud boundaries or including subadiabatic parcels that have been subjected to inhomogeneous mixing processes. Thus method 2 screening omits low LWC observations, so that variance in ln (CDNC) is less than the variance in ln ($\langle d^3\rangle$). In this manner, those observations having the maximum LWC at each pass are selected, irrespective of the adiabatic prediction.

[11] Most often, droplet concentrations derived using method 2 are larger than those derived using method 1. Two explanations are suggested below. Typically, there is a range of humidity beneath each cloud that produces variability in the adiabatic LWC profile. The source for this range is that air entering cloud base is not undiluted boundary layer air, but rather is a varying mixture of boundary layer air and lower tropospheric air that is typically drier and warmer, which often has different aerosol properties. If the subcloud measurements are somehow biased toward drier air because of limited sampling statistics, then the computed adiabatic LWC will be biased low. Because inhomogeneous mixing processes dominate over homogeneous mixing processes in these cloud regions, this bias would produce lower measured droplet concentrations. On the other hand, the range in LWC within the screened data may be a direct consequence of the variability in subcloud humidity. Higher-humidity parcels may be associated with stronger updrafts that originated closer to the surface, which is a source of moisture, buoyancy, and CCN. This may explain the strong positive correlation between updraft velocity and CDNC that was often observed near cloud bases. Because it is not clear from the present measurements whether method 1 or method 2 more accurately isolates adiabatic parcels, each method will be used, and differences will be interpreted as due to experimental uncertainty.

[12] The aerosol-CDNC closure for 20 of the clouds using method 1 screening is shown in Figure 2. A linear fit to the data (dashed line) has a slope of 1.03. The slope is statistically indistinguishable from unity, and the mean percent deviation is −12% with a standard deviation about the mean of 13%. The mean underprediction is comparable to the uncertainty in the measured number concentration. The standard deviation is comparable to the variability in

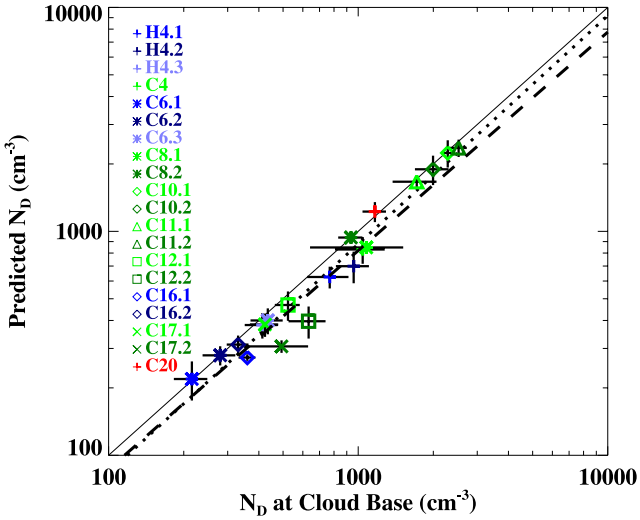

Figure 2. Aerosol-CDNC closure: predicted versus observed droplet concentration. Observed values use method 1 screening (see text) for adiabaticity. The short-dashed line represents an unweighted least squares linear fit to the data in log-log units. The long-dashed line represents a fit to the data when method 2 screening is used. The solid line represents perfect model-observation agreement. The term "cloud base" reiterates that observations used in this plot were generally taken in adiabatic regions within 100 m of cloud base.

the DACADS concentration used as input to the model. There is no statistically significant correlation between the modeled-observed CDNC difference and the following quantities: OC:SO_4^{2-} mass concentration ratio, modeled-measured CCN concentration, updraft velocity, updraft velocity variance, or total droplet concentration. While these factors may influence the model-observation difference (as discussed in sections 4 and 5), their combined effect does not exceed the experimental noise. Also shown in Figure 2 is the linear fit of the model predictions to method 2 data. This can be considered a range of uncertainty related to the method used to differentiate adiabatic parcels from subadiabatic parcels. The slope using method 2 is still indistinguishable from unity at 0.98. The mean deviation is larger at −16%, with a standard deviation about the mean of 15%.

[13] The difference between methods 1 and 2 of 4% combined with the 15% uncertainty in the CAS concentration measurement yields an estimated 16% uncertainty in the measured cloud base concentration. Uncertainty in modeled cloud drop concentration is 10% from a contribution of uncorrelated uncertainties: 5% from aerosol concentration, 0.5% from DACADS sizing uncertainty, 8% from updraft velocity uncertainty, and 5% from parcel modeling simplifications. Uncertainty in modeled values of CDNC is thus 11%. This yields a net experimental uncertainty of 20% in the model-observation comparison. The mean model-observation bias taking an average of methods 1 and 2 for observed concentration is −14%. This bias is within the estimated experimental uncertainty. We note that the model assumes that aerosol composition is pure ammonium bisulfate, which is not entirely consistent with the observed composition and hygrosocopic data presented in section 4. The effect of varying the ammonium bisulfate assumption on the model-observation closure is discussed in section 5.

3. Effects of Aerosol on the Vertical Profile of Cloud Microphysics

[14] A more comprehensive description of cloud microphysics must include the effects of entrainment mixing, as adiabatic parcel model predictions are only useful in regions where there is little or no mixing among parcels of differing histories. Outside of these "adiabatic cores," entrainment mixing alters droplet concentrations, size distribution, LWC, and cloud thermodynamics via complex and unresolved mechanisms. Cloud albedo and precipitation efficiency are very sensitive to both cloud drop concentration and the shape of the size distribution; thus it will be useful to investigate the apparent relationships between aerosol, cloud drop concentration, and size distribution in subadiabatic cloud regions.

[15] At the core of these uncertainties is the observation that the dispersion in the cloud drop size distribution generally exceeds that of model predictions. Likewise, dispersion tends to be greater in polluted clouds than in unpolluted clouds [*McFarquhar and Heymsfield*, 2001]. It is not clear whether this increase is due to activation of entrained aerosol [*Bower and Choularton*, 1988], activation of interstitial aerosol within vertically accelerating parcels [*Segal et al.*, 2003], differential droplet growth rates due to chemical differences among droplets [*Liu and Daum*, 2002; *Feingold and Chuang*, 2002], or multiphase flow processes such as enhanced coalescence or supersaturation due to vortex spin-out [*Shaw*, 2003].

[16] To illustrate the large effect of aerosol on the vertical profile of cloud properties, two extreme examples from

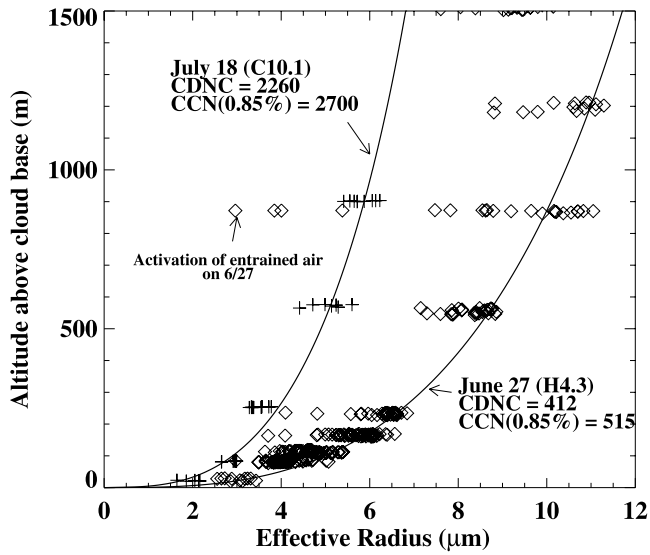

Figure 3. CCN-forced variations in CDNC and influence on the vertical profile of effective radius. The stated CCN and CDNC values for each cloud were obtained below cloud and within 100 m of cloud base, respectively. Solid lines are adiabatic predictions using observed subcloud thermodynamic properties and observed CDNC within 50 m of cloud base.

27 June (H4.3) and 18 July (C10.1) are shown in Figure 3 with their respective adiabatic calculations. For each cloud both peak effective radius and peak droplet concentrations maintained nearly adiabatic values through the lowest ~1 km of the cloud core. H4.3 exhibited an adiabatic core 1200 m above cloud base, whereas C10.1 appeared to be more strongly influenced by entrainment, with adiabatic LWC values only in the lowest pass.

[17] A variety of phenomena, including bimodal spectra, activation of entrained CCN, and evidence for a mixture of both homogeneous and inhomogeneous mixing processes, was observed from profiles taken in this study. For example, the points identified in Figure 3 as "activation of entrained air" in cloud H4.3 were characterized by high droplet concentrations, narrow size spectra, and small effective radii and were found within a strong updraft 900 m above cloud base. These features are identical to those of recently activated parcels found near cloud base and are inconsistent with microphysical properties found in detraining, evaporating cloud parcels, which characteristically have broad dispersions and low concentrations. Likewise, the subadiabatic profile of LWC in C10.1 was accompanied by a positive gradient in droplet dispersion strong enough to maintain nearly adiabatic profiles of effective radius and droplet concentration. An in-depth evaluation of these phenomena is beyond the scope of this work, yet deserves further study given the array of instrumentation directed toward aerosol and cloud microphysical characterization.

4. Relationships Among Hygroscopic Growth, CCN, and Organic Carbon

[18] In section 2, the model assumed that CCN are composed of simple salts. In this section, we examine this assumption using observations of organic carbon and sulfate mass concentrations, hygroscopic growth, and CCN properties. These observations were made on the Twin Otter aircraft with relatively rapid time resolution (5 min for composition) and thus can be used to capture variability in aerosol properties during a single flight.

[19] It is widely acknowledged that the hygroscopic properties of organic carbon (OC) aerosol vary among differing species and that OC aerosols generally behave differently from inorganic salts. Two important quantities relevant to OC hygroscopic properties are explored here: First is hygroscopic growth (defined below); second is critical supersaturation/CCN concentration. Compared with sulfate aerosol of the same dry diameter, OC aerosol generally produces fewer dissolved species per unit volume. This effect leads to smaller hygroscopic growth and higher critical supersaturation. Certain species of OC can even be insoluble and hydrophobic. In contrast, surface active OC species (especially humics) have been found to reduce surface tension, hence decreasing the critical supersaturation of the aerosol relative to the case in which surface tension is not reduced [*Facchini et al.*, 1999]. The effect of surface tension reduction is less apparent on hygroscopic growth, being noticeable only at small (<100 nm) sizes. When OC is found in the same aerosol population as inorganic salts, such as sulfate, the degree to which these species are internally mixed within individual particles plays an important role in the aggregate hygroscopic properties of the aerosol population.

[20] In light of these complicated and competing effects and the currently poor ability to speciate atmospheric organics, there is a need for observations to constrain the hygroscopic properties of OC-containing aerosol populations in various regions. Some insight into this behavior for the organic species observed during CRYSTAL-FACE is obtained and presented here using three measurements: the DACADS, which measures aerosol size distribution at dry (15–20%) and moist (50–75%) relative humidities (RH); the Caltech CCN counter, measuring concentration of aerosol having critical supersaturations below 0.85%, and the AMS measurement of OC and SO_4^{2-} mass concentrations.

[21] The hygroscopic growth factor of a particle $f(\mathrm{RH})$ is defined as the ratio of its equilibrium diameter $D(\mathrm{RH})$ at a specified relative humidity RH to its dry diameter d: $f(\mathrm{RH}) = D(\mathrm{RH})/d$. In an arbitrary aerosol population, particles of a fixed dry size will have varying composition and hence varying values of $f(\mathrm{RH})$. The ideal instrument to measure $f(\mathrm{RH})$ as a function of d is the tandem differential mobility analyzer (DMA), in which the distribution of $f(\mathrm{RH})$ values is obtained for each dry size d [e.g., *Brechtel and Kreidenweis*, 2000]. Given current instrument configurations, this measurement takes a prohibitively long time for aircraft sampling, during which aerosol properties would be varying considerably. In contrast to the tandem DMA, the DACADS used on the Twin Otter obtains size distributions from two identical DMA columns operating at different relative humidities. This method provides more limited information, in that the effect of chemical heterogeneities at each size is not obtained, but has the distinct advantage that complete size distributions are obtained every 100 s. An effective value of $f(\mathrm{RH})$ is obtained from the DACADS data as a function of d using two methods (Figures 4a and 4b). The first method simply calculates the required (nonuniform) shift in diameter of the dry size distribution to reproduce the moist size distribution (Figure 4b). This method is subject to uncertainties related to differences in the size-dependent loss rates and calibration uncertainties between the dry and humid DMA columns. The second method takes advantage of the fact that most size distributions exhibit distinct Aitken and accumulation size modes, each of which shifts coherently with relative humidity (Figure 4a). In the second procedure both the dry and humid size distributions are represented as two or three lognormal modes using a least squares fitting technique. An effective $f(\mathrm{RH})$ is determined for Aitken and accumulation modes separately on the basis of the shift in mode diameter. Changes in the width of the mode may be due to chemical heterogeneity within the population. This method provides less information than method 1, but does not suffer from size-dependent calibration and loss uncertainties as long as such uncertainties are slowly varying with size. To reduce sampling noise, each of the 11 days used in this study is subdivided into 2–6 periods representing distinct atmospheric conditions (altitude range, over land versus over sea, presence or lack of significant concentrations of <30-nm particles). All DACADS size distributions made within each period

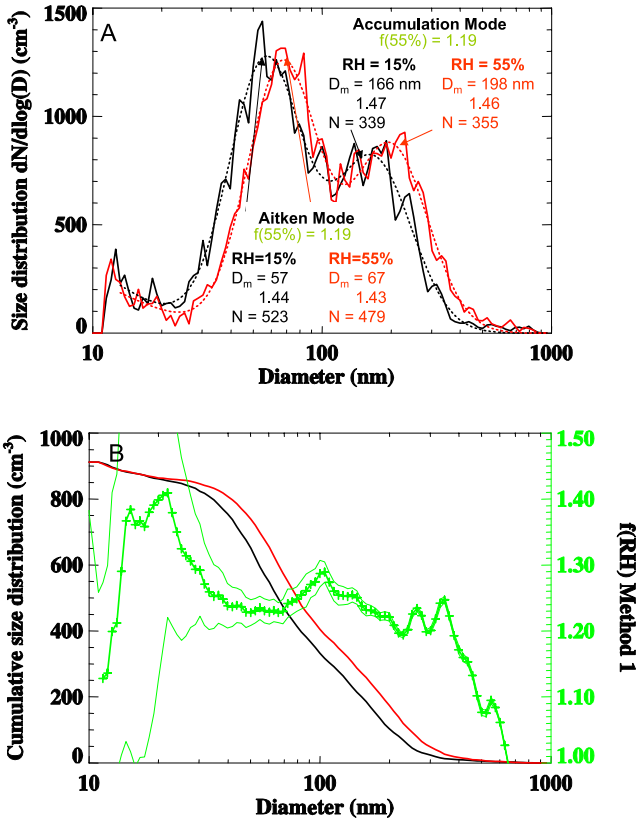

Figure 4. Illustration of methods 1 and 2 (see text) for determining hygroscopic growth factor from the DACADS data. (a) Dry and humid (55% RH) size distribution for measurements below 800-m altitude in the vicinity of clouds H4.1 and H4.2. The lognormal fitting is shown as dashed lines. The fitted parameters and method 2 f(RH = 55%) values are shown for each mode. (b) Cumulative size distributions from Figure 4a above, plotted as a function of dry diameter with the method 1 hygroscopic growth factor. Truncation in the size distribution limits accuracy beyond 300 nm.

are averaged together before being analyzed for hygroscopic growth. To minimize the occurrence of cases in which the humid column is not sufficiently moist to deliquesce particles that were dry in the atmosphere, only observations with ambient RH > 60% are considered.

[22] To relate observed hygroscopic growth factors to observed CCN concentrations, an effective cutoff diameter D_C(0.85%) is obtained from the CCN(0.85%) concentration and the dry DACADS size distribution. D_C(0.85%) is defined such that

$$\mathrm{CCN}(0.85\%) = \int_{D_C(0.85\%)}^{800\ \mathrm{nm}} N(d)\mathrm{d}d,$$

where $N(d)$ is the DACADS-measured dry size distribution. For an aerosol population composed completely of ammonium sulfate, D_C (0.85%) would be approximately 32 nm. Less hygroscopic species would exhibit larger values of D_C(0.85%). For the observations presented here, D_C (0.85%) ranges from 20 to 60 nm, which generally falls within the Aitken mode. Thus the hygroscopic properties found at Aitken mode size ranges will be most relevant to the CCN(0.85%) closure. Figure 5a illustrates the relationship between f(RH) of the Aitken mode to D_C(0.85%). Only cases in which method 1 and method 2 agree within 10% are included in the analysis. Variability in humid RH (which ranged from 50% to 75%) is a source of uncertainty in the following analyses (Figure 5b). The weak correlation between RH and f(RH) among the data used in this study indicates a small effect of RH variability relative to that of aerosol composition. The relationship between Aitken mode hygroscopic growth and D_C(0.85%) suggests that compositional variations are influencing both hygroscopic growth and critical supersaturation in a consistent manner. Data

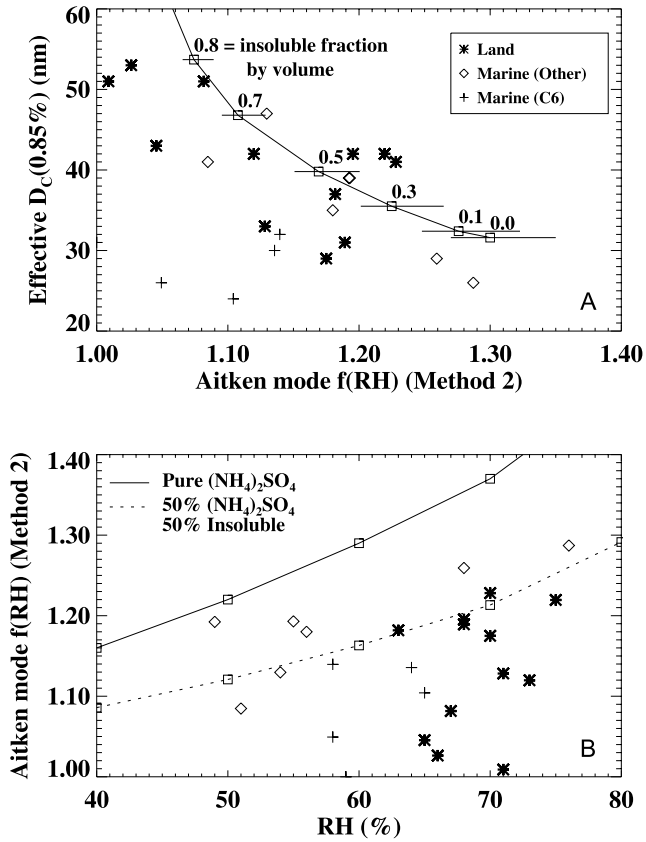

Figure 5. (a) Effective cutoff diameter for S_C = 0.85% plotted versus f(RH) for the Aitken mode using method 2. Diamonds are overland flights, asterisks are marine flights, and pluses are data from the marine flight C6 (discussed in text). Model simulations for $(NH_4)_2SO_4$ mixed internally with the indicated volume fraction of insoluble material are shown as connected squares. The f(RH) in the model calculations curve corresponds to 63% RH, and the range bars represent values from 59% to 69% (median values for ocean and land, respectively). (b) The f(RH) plotted versus humid DMA RH for the same points as in Figure 5a. The curves correspond to uncrystallized $(NH_4)_2SO_4$. The solid curve represents pure sulfate, and the dashed curve represents sulfate internally mixed with an equal volume of insoluble material (50% OC by volume would correspond to about 35% OC by mass).

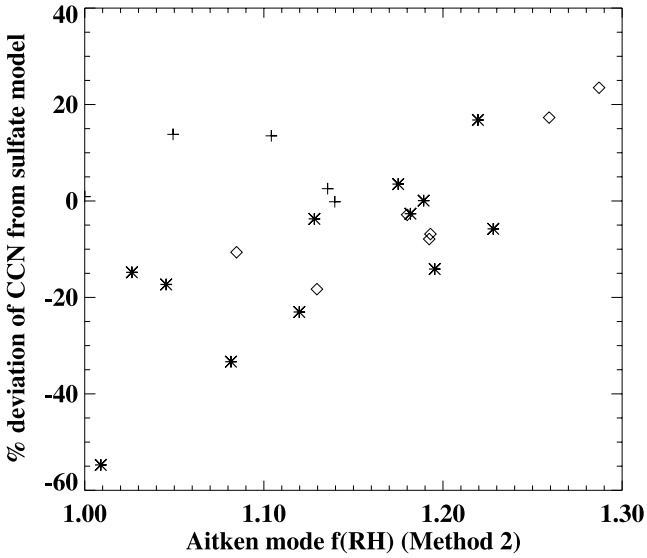

Figure 6. Percent difference between observed CCN(0.85%) and $N(d > 32$ nm) obtained from the DMA plotted as a function of f(RH) of the Aitken mode. Symbols are the same as those in Figure 5.

from marine flight C6 (10 July) are shown separately in Figures 5a and 5b, since the simultaneously low D_C(0.85%) and f(RH) values are unique. Sea salt has a very low activation diameter (D_C(0.85%) = 25 nm) and may not have been deliquesced in the humid DMA, which was operating near the NaCl crystallization point of 62% RH. It is conceivable that small sea-salt particles contributed significantly to the Aitken mode concentrations on this flight (the open sea wind speed at 50-m altitude ranged from 7 to 12 m s^{-1}), although fine sea-salt concentrations in excess of 100 cm^{-3} exceed even the surf zone observations of *Clarke et al.* [2003].

[23] Overlain on Figure 5a is the relationship between D_C(0.85%) and f(RH) obtained from model calculations assuming an internal mixture of ammonium sulfate solution and insoluble material. The curve corresponds to RH = 63%, and the horizontal bars represent the effect of varying RH from 59% to 69% in the f(RH) calculation. Two model curves are shown for Figure 5b to illustrate the expected f(RH) for pure ammonium sulfate aerosol and that for a 50/50 volumetric mix of sulfate and insoluble material (e.g., 35% OC by mass).

[24] While D_C(0.85%) is more uniquely related to composition than CCN concentration, it is relevant to examine the relationships between hygroscopic growth and CCN concentration to bound the effect variations in hygroscopic growth have on CCN(0.85%). Figure 6 illustrates the percent difference between observed CCN(0.85%) to that predicted assuming the DACADS dry size distribution assuming ammonium sulfate (i.e., D_C(0.85%) = 32 nm), plotted versus f(RH). The variability in CCN concentration falls within the range of −30% to +20%, with one outlier approaching −60% (from C20), and this variability is clearly associated with the hygroscopic growth factor for the Aitken mode.

[25] Last, we explore the relationship between OC and hygroscopic behavior. D_C(0.85%) is plotted versus the ratio of OC:SO_4^{2-} mass concentrations observed by the AMS for 100–600-nm diameter particles in Figure 7. Two regimes exist. In the first regime, where OC:SO_4^{2-} mass ratio is <0.5, a very weak relationship exists between CCN cutoff diameter and OC fraction, despite a large variability in D_C(0.85%). In the second regime, for which OC:SO_4^{2-} > 0.5, cutoff diameter increases with increasing OC fraction, indicative of the expected lower hygroscopicity of OC species. The majority of these high-OC:SO_4^{2-} observations were made on flights C10 and C11 (18 July 2002). Backward Lagrangian trajectories computed from the National Oceanic and Atmospheric Administration (NOAA) Hybrid Single-Particle Lagrangian Integrated Trajectory (HYSPLIT) [*Draxler*, 1999] model for this day estimate that the air mass below 2000 m resided over the Florida peninsula for over 48 hours in a slow, southerly flow. This contrasts with the other days studied here, in which the air masses resided over land for less than 24 hours. An interesting relationship between OC and f(RH) appears for the cases when OC:SO_4^{2-} < 0.5 (Figure 8a). There is a general decrease in the hygroscopic behavior of the Aitken mode when OC fractions increase from 0.1 to 0.5. An interpretation of this result must take into account that the bulk of AMS mass is taken from sizes larger than those in the Aitken mode and that the accumulation mode shows a much weaker relationship between hygroscopic growth and OC:SO_4^{2-} ratio relative to the Aitken mode (Figure 8b). These results imply that OC plays a strong role in Aitken mode hygroscopicity and a weaker role in accumulation mode hygroscopicity. These observations are consistent with accumulation mode particles being internal mixtures of OC and SO_4^{2-}.

[26] Despite the relationships seen among f(RH), D_C(0.85%), and OC:SO_4 mass ratios, there is no statistically significant correspondence between each of these three observations and the degree of aerosol-CDNC closure. The first three quantities are measured in longer (6–60 min) out-of-cloud periods, which allows for much reduced sampling uncertainty, whereas CDNC and updraft velocity are taken from relatively shorter (tens of seconds) sampling periods within cloud base regions. Despite this increase in sampling uncertainty, it is notable that the standard deviation between the observations and the mod-

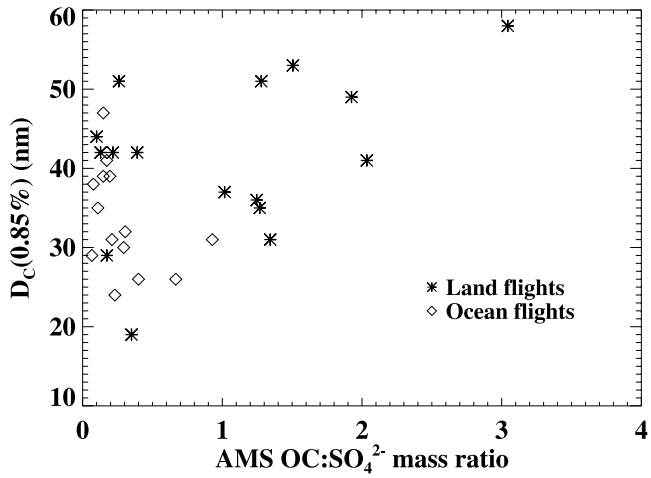

Figure 7. Relationship between D_C(0.85%) and AMS-measured organic carbon to sulfate mass ratio.

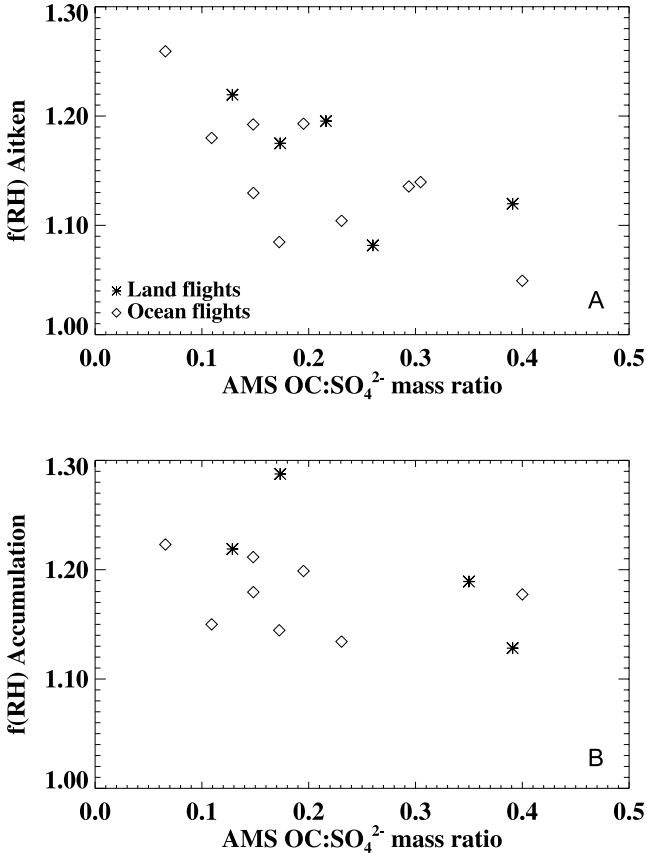

Figure 8. (a) Relationship between Aitken mode f(RH) and AMS-measured organic carbon to sulfate mass ratio for OC:SO_4^{2-} ratios below 0.5. (b) Same as Figure 8a, but for accumulation mode f(RH).

els of CDNC is of order 15%. This suggests that the range of variation in CCN concentration that is related to aerosol hygroscopicity (Figure 6) is an upper limit on the influence composition has on CDNC in this study.

5. Discussion

[27] To summarize, cloud drop concentrations in Florida cumulus were observed to vary from 300 cm^{-3} to 2300 cm^{-3}, and this is driven primarily by large variations of CCN concentration in this region. The effects of the boundary layer aerosol on cloud microphysics persist through at least the lowest 1 km of the clouds. An aerosol-CDNC closure is obtained between predicted and observed CDNC with a bias within the experimental uncertainty of 20% and variability in model-observation agreement within ~15%, which is comparable to that expected because of experimental sampling limitations. The above closures assume ammonium bisulfate aerosol composition. The CCN closure exhibits variability with a 17% standard deviation, which is found to be related to composition, as inferred from the observed hygroscopic growth and the organic carbon to sulfate mass ratio.

[28] We can now ask two questions. (1) Given the 14% model-observation agreement for aerosol-CDNC closure and the 10–20% agreement for aerosol-CCN closure found by *VanReken et al.* [2003], what constraints do these observations place on assumptions entering the models? (2) What are the most important elements for the complete aerosol-CCN-cloud closure, and are there simplifications that can be used in aerosol activation models for this region?

5.1. Question 1

[29] Table 3 illustrates the sensitivity of CCN and CDNC to variations in certain key modeling assumptions. Table 3 values are derived for two specific test cases here, but are consistent with the analyses of *Roberts et al.* [2002], *VanReken et al.* [2003], and *Rissman et al.* [2004]. Two quite different cases are chosen as examples, one from the relatively clean marine case on 10 July and the other from one of the most polluted cases on 18 July. The baseline case corresponds to ammonium bisulfate aerosol, condensation coefficient of 0.06, surface tension of water, no soluble gases, and updraft velocity of 2 m s^{-1}. The accuracy of the CDNC sensitivity tests is ±2% because of the size resolution used in the parcel model. The CDNC sensitivity to varying sulfate type (rows 1 and 2 in Table 3) may have somewhat larger uncertainties (~5%) due to simplifications in the parcel model's treatment of sulfate water activity.

[30] The effect of varying modeling assumptions on the CCN spectrum is comparable to the 17% root-mean-square variability in aerosol-CCN closure shown in section 4 and by *VanReken et al.* [2003]. Thus the CCN data do not rule out moderate variations in the chemical assumptions used.

Table 3. Effects of Changing Model Assumptions on Predicted CCN and CDNC[a]

	CCN 0.2%		CCN 0.85%		CDNC	
	C10.1	C6.1	C10.1	C6.1	C10.1	C6.1
$(NH_4)_2SO_4$	−1.5%	−1.2%	−0.2%	−0.9%	+4%	+5%
H_2SO_4[b]	−15%	−13%	−3%	−10%	−13%	−24%
50% insoluble (externally mixed)	−50%	−50%	−50%	−50%	−28%	−41%
50% insoluble (internally mixed)	−23%	−21%	−5%	−19%	−5%	−15%
20% surface tension reduction	+18%	+19%	+5%	+15%	+8%	+11%
50% insoluble (internal) and 20% surface tension reduction	−2%	−1%	0%	−1%	+4%	+0%
Updraft + 0.35 m s^{-1}	ND	ND	ND	ND	+8%	+5%
Condensation coeff. = 0.03	ND	ND	ND	ND	+11%	+10%
Condensation coeff. = 0.3	ND	ND	ND	ND	−9%	−10%

[a]See text. ND, not a model-dependent parameter.
[b]The sulfuric acid calculations include 35% H_2O by weight to the dry size distribution because of the fact that "dry" aerosol size distribution is measured at 15–20% RH. The other sulfate species are assumed to be crystallized below 20% RH.

The values in Table 3 should be interpreted keeping in mind that predicted CDNC using ammonium bisulfate is, on average, ~15% lower than the observations, which is still within the estimated experimental uncertainty of 20%. The −15% bias in the baseline model-observation difference is opposite to that expected from the neglect of species less soluble than ammonium bisulfate. For example, if one were to infer from the median value of f(RH) shown in Figure 5 that the insoluble fraction was ~50%, then model observation bias would further decrease by approximately 10%. This would increase model-observation bias beyond the estimated experimental uncertainties. Note that the inference of insoluble fraction from the f(RH) data presented in section 4 is associated with large uncertainties, and this result should not be overinterpreted. Both the CCN and the CDNC closures suggest smaller insoluble fractions. However, it is significant that the sign of this discrepancy contrasts with some previous studies, in which a larger-than-measured insoluble fraction was needed in order to obtain closure (see review given by *VanReken et al.* [2003]). Moreover, the sign and magnitude of the model-observation discrepancy support the lower values of water condensation coefficient (~0.06) that have been used over the previous 50 years, as higher values (~0.3 or greater) would increase the model-observation difference beyond the estimated uncertainties.

5.2. Question 2

[31] *Twomey* [1959] derived a simple analytical approximation to obtain droplet concentration from updraft velocity and a two-parameter fit to the CCN spectrum, $\mathrm{CCN}(S) = CS^k$,

$$\mathrm{CDNC} = C^{2/(k+2)}\left[\frac{cw^{3/2}}{kB(k/2, 3/2)}\right]^{k/(k+2)}, \qquad (1)$$

where w is updraft velocity, B is the beta function, and c is a constant that depends on initial parcel thermodynamic state and aerosol chemical properties. In contrast, the parcel model used in the present study performs a detailed numerical integration of the growth equation, where a 200-bin size distribution is derived from a 4-mode lognormal fit to the data, and droplet growth is derived from complete Köhler theory, as opposed to just the supersaturation spectrum. Given the wide range of conditions encountered during CRYSTAL-FACE, it is interesting to test how much added predictive ability is achieved by using the more detailed calculations. To address this, a series of calculations are made using equation (1), which are then compared to the more detailed parcel model calculations. First, the parameters C and k are taken from model-derived CCN concentrations at 0.2% and 0.85%, and w is taken from the measurements. The small, but finite, 7% standard deviation between the simple Twomey approximation and the detailed calculations is presumably caused by the simplicity of the Twomey expression. Next, the Twomey equation is used as a tool to test which parameters controlled droplet concentration during CRYSTAL-FACE. First, the simplest assumption is taken, in which CCN at 0.85% concentration is the only model input from observations; k is fixed at 0.8 (a common assumption), and updraft velocity is fixed at 2 m s^{-1}. The standard deviation between the detailed model and this simple case is 15%. Thus CCN at 0.85% together with representative, but fixed, values of updraft velocity and spectral shape match detailed droplet concentration calculations to within 15%. Introducing observed values of k (which range from 0.32 to 0.85) drops the standard deviation only to 13%. Introducing measured updraft velocity with fixed k improves this to 8%, and introducing measured w and k improves the situation marginally to within 7%. When comparing the Twomey model to observations, considering only CCN at 0.85% leaves a variability of 18%, while the full Twomey equation leaves only 13% of the signal unexplained, which is the same as when observations are compared to the detailed model.

[32] In conclusion, this study and that of *VanReken et al.* [2003] have obtained closure among simultaneous measurements of aerosol physical properties, CCN concentrations, cloud drop concentrations, and models that use simple chemistry within the experimental accuracy of ~20%. The degree of closure of 20% in this subtropical region with urban and maritime influences rules out any anomaly of the magnitude reported by some previous studies (see review given by *VanReken et al.* [2003]) that were conducted in different regions. Previous studies may have been influenced by differing aerosol compositions among the regions, differing cloud dynamics, and different measurement and analysis techniques. The degree of closure is not sufficiently precise to constrain certain chemical effects on cloud activation that have magnitudes less than 20% (Table 3). This study provides hope that future measurements using similar closure strategies together with improved experimental techniques will afford better accuracy in understanding aerosol-cloud interactions.

[33] **Acknowledgment.** This work was supported by National Aeronautics and Space Administration grant NAG5-11549 and the Office of Naval Research.

References

Ackerman, A. S., O. B. Toon, J. P. Taylor, D. W. Johnson, P. V. Hobbs, and R. J. Ferek (2000), Effects of aerosols on cloud albedo: Evaluation of Twomey's parameterization of cloud susceptibility using measurements of ship tracks, *J. Atmos. Sci.*, *57*, 2684–2695.

Albrecht, B. A. (1989), Aerosols, cloud microphysics, and fractional cloudiness, *Science*, *245*, 1227–1230.

Baumgardner, D., W. Strapp, and J. E. Dye (1985), Evaluation of the Forward Scattering Spectrometer Probe. Part II: Corrections for coincidence and dead-time losses, *J. Atmos. Oceanic Technol.*, *2*, 626–632.

Baumgardner, D., H. Jonsson, W. Dawson, D. O'Connor, and R. Newton (2001), The cloud, aerosol and precipitation spectrometer: A new instrument for cloud investigations, *Atmos. Res.*, *59–60*, 251–264.

Bower, K. N., and T. W. Choularton (1988), The effects of entrainment on the growth of droplets in continental cumulus clouds, *Q. J. R. Meteorol. Soc.*, *114*, 1411–1434.

Brechtel, F. J., and S. M. Kreidenweis (2000), Predicting particle critical supersaturation from hygroscopic growth measurements in the humidified TDMA. Part I: Theory and sensitivity studies, *J. Atmos. Sci.*, *57*, 1854–1871.

Burnet, F., and J.-L. Brenguier (2002), Comparison between standard and modified forward scattering spectrometer probes during the small cumulus microphysics study, *J. Atmos. Oceanic Technol.*, *19*, 1516–1531.

Chuang, P. Y., D. R. Collins, H. Pawlowska, J. R. Snider, H. H. Jonsson, J. L. Brenguier, R. C. Flagan, and J. H. Seinfeld (2000), CCN measurements during ACE-2 and their relationship to cloud microphysical properties, *Tellus, Ser. B*, *52*, 842–866.

Clarke, A., V. Kapustin, S. Howell, K. Moore, B. Leinert, S. Masonis, T. Anderson, and D. Covert (2003), Sea-salt size distributions from breaking waves: Implications for marine aerosol production and optical extinction measurements during SEAS, *J. Atmos. Oceanic Technol.*, *20*, 1362–1374.

Draxler, R. R. (1999), Hybrid Single-Particle Lagrangian Integrated Trajectories (HY-SPLIT), version 4.0: Users guide, *NOAA Tech. Memo. ERL ARL-230*, 35 pp., Natl. Oceanic and Atmos. Admin., Silver Spring, Md.

Dye, J. E., and D. Baumgardner (1984), Evaluation of the Forward Scattering Spectrometer Probe, *J. Atmos. Oceanic Technol.*, *1*, 329–344.

Facchini, M. C., M. Mircea, S. Fuzzi, and R. J. Charlson (1999), Cloud albedo enhancement by surface-active organic solutes in growing droplets, *Nature*, *401*, 257–259.

Feingold, G., and P. Chuang (2002), Analysis of the influence of film-forming compounds on droplet growth: Implications for cloud microphysical processes and climate, *J. Atmos. Sci.*, *59*, 2006–2018.

Fitzgerald, J. W., and P. Spyers-Duran (1973), Changes in cloud nucleus concentration and cloud droplet size distribution associated with pollution from St. Louis, *J. Appl. Meteorol.*, *30*, 511–516.

Gysel, M., E. Weingartner, S. Nyeki, D. Paulsen, U. Baltensperger, I. Galambos, and G. Kissn (2004), Hygroscopic properties of water-soluble matter and humic-like organics in atmospheric fine aerosol, *Atmos. Chem. Phys.*, *4*, 35–50.

Houghton, J. T., Y. Ding, D. J. Griggs, M. Noguer, P. J. van der Linden, X. Dai, K. Maskell, and C. A. Johnson (Eds.) (2001), *Climate Change 2001: The Scientific Basis, Contribution of Working Group I to the Third Assessment Report of the Intergovernmental Panel on Climate Change*, 881 pp., Cambridge Univ. Press, New York.

Kreidenweis, S. M., C. J. Walcek, G. Feingold, W. Gong, M. Z. Jacobson, C. H. Kim, X. Liu, J. E. Penner, A. Nenes, and J. H. Seinfeld (2003), Modification of aerosol mass and size distribution due to aqueous-phase SO_2 oxidation in clouds: Comparisons of several models, *J. Geophys. Res.*, *108*(D7), 4213, doi:10.1029/2002JD002697.

Laaksonen, A., P. Korhonen, M. Kulmala, and R. J. Charlson (1998), Modification of the Köhler equation to include soluble trace gases and slightly soluble substances, *J. Atmos. Sci.*, *55*, 853–862.

Lawson, R. P., and A. M. Blyth (1998), A comparison of optical measurements of liquid water content and drop size distribution in adiabatic regions of Florida cumuli, *Atmos. Res.*, *48*, 671–690.

Lenschow, D. H. (1986), Aircraft measurements in the boundary layer, in *Probing the Atmospheric Boundary Layer*, edited by D. H. Lenschow, pp. 39–55, Am. Meteorol. Soc., Boston, Mass.

Liu, Y. G., and P. H. Daum (2002), Anthropogenic aerosols: Indirect warming effect from dispersion forcing, *Nature*, *419*, 580–581.

McFarquhar, G. M., and A. J. Heymsfield (2001), Parameterizations of INDOEX microphysical measurements and calculations of cloud susceptibility: Applications for climate studies, *J. Geophys. Res.*, *106*, 28,675–28,698.

Nenes, A., and J. H. Seinfeld (2003), Parameterization of cloud droplet formation in global climate models, *J. Geophys. Res.*, *108*(D14), 4415, doi:10.1029/2002JD002911.

Nenes, A., R. J. Charlson, M. C. Facchini, M. Kulmala, A. Laaksonen, and J. H. Seinfeld (2002), Can chemical effects on cloud droplet number rival the first indirect effect?, *Geophys. Res. Lett.*, *29*(17), 1848, doi:10.1029/2002GL015295.

Prenni, A. J., P. J. De Mott, and S. M. Kreidenweis (2003), Water uptake of internally mixed particles containing ammonium sulfate and dicarboxylic acids, *Atmos. Environ.*, *37*, 4232–4251.

Pruppacher, H. R., and J. D. Klett (1997), *Microphysics of Clouds and Precipitation*, 2nd rev., 954 pp., Kluwer Acad., Norwell, Mass.

Rissman, T. A., A. Nenes, and J. H. Seinfeld (2004), Chemical amplification (or dampening) of the Twomey effect: Conditions derived from droplet activation theory, *J. Atmos. Sci.*, *61*, 919–930.

Rivera-Carpio, C. A., C. E. Corrigan, T. Novakov, J. E. Penner, C. F. Rogers, and J. C. Chow (1996), Derivation of contributions of sulfate and carbonaceous aerosols to cloud condensation nuclei from mass size distributions, *J. Geophys. Res.*, *101*, 19,483–19,493.

Roberts, G. C., P. Artaxo, J. Zhou, E. Swietlicki, and M. O. Andreae (2002), Sensitivity of CCN spectra on chemical and physical properties of aerosol: A case study from the Amazon Basin, *J. Geophys. Res.*, *107*(D20), 8070, doi:10.1029/2001JD000583.

Rosenfeld, D., and I. M. Lensky (1998), Satellite-based insights into precipitation formation processes in continental and maritime convective clouds, *Bull. Am. Meteorol. Soc.*, *79*, 2457–2476.

Segal, Y., M. Pinsky, A. Khain, and C. Erlick (2003), Thermodynamic factors influencing bimodal spectrum formation in cumulus clouds, *Atmos. Res.*, *66*, 43–64.

Shaw, R. A. (2003), Particle-turbulence interactions in atmospheric clouds, *Annu. Rev. Fluid Mech.*, *35*, 183–227.

Shaw, R. A., and D. Lamb (1999), Experimental determination of the thermal accommodation and condensation coefficients of water, *J. Chem. Phys.*, *111*, 10,659–10,663.

Shulman, M. L., M. C. Jacobson, R. J. Charlson, R. E. Synovec, and T. E. Young (1996), Dissolution behaviour and surface tension effects of organic compounds in nucleating cloud droplets, *Geophys. Res. Lett.*, *23*, 277–280.

Snider, J. R., and J.-L. Brenguier (2000), Cloud condensation nuclei and cloud droplet measurements during ACE-2, *Tellus, Ser. B*, *52*, 828–842.

Snider, J. R., S. Guibert, J.-L. Brenguier, and J. P. Putaud (2003), Aerosol activation in marine stratocumulus clouds: 2. Kohler and parcel theory closure studies, *J. Geophys. Res.*, *108*(D15), 8629, doi:10.1029/2002JD002692.

Twomey, S. (1959), The nuclei of natural cloud formation. Part II: The supersaturation in natural clouds and the variation of cloud droplet concentration, *Geofis. Pura Appl.*, *43*, 243–249.

Twomey, S. (1977), The influence of pollution on the shortwave albedo of clouds, *J. Atmos. Sci.*, *34*, 1149–1152.

Twomey, S., and J. Warner (1967), Comparison of measurements of cloud droplets and cloud nuclei, *J. Atmos. Sci.*, *24*, 702–703.

VanReken, T. M., T. A. Rissman, G. C. Roberts, V. Varutbangkul, H. H. Jonsson, R. C. Flagan, and J. H. Seinfeld (2003), Toward aerosol/cloud condensation nuclei (CCN) closure during CRYSTAL-FACE, *J. Geophys. Res.*, *108*(D20), 4633, doi:10.1029/2003JD003582.

R. Bahreini and W. C. Conant, Department of Environmental Science and Engineering, California Institute of Technology, 1200 E. California Boulevard, Pasadena, CA 91125, USA. (broya@caltech.edu; billc@cheme.caltech.edu)

A. E. Delia, Program in Atmospheric and Oceanic Sciences, University of Colorado, UCB 311, Boulder, CO 80309-0311, USA. (alice.delia@colorado.edu)

R. C. Flagan, T. A. Rissman, J. H. Seinfeld, T. M. VanReken, and V. Varutbangkul, Chemical Engineering, California Institute of Technology, Mail Code 210-41, 1200 E. California Boulevard, Pasadena, CA 91125, USA. (flagan@caltech.edu; rissman@its.caltech.edu; seinfeld@caltech.edu; vanreken@its.caltech.edu; tomtor@its.caltech.edu)

J. L. Jimenez, Department of Chemistry and Biochemistry, Cooperative Institute for Research in Environmental Sciences, University of Colorado, UCB 216, Boulder, CO 80309-0216, USA. (jose.jimenez@colorado.edu)

H. H. Jonsson, CIRPAS, Naval Postgraduate School, 3240 Imjin Road, Range 510, Monterey, CA 93633, USA. (hjonsson@nps.navy.mil)

A. Nenes, Schools of Earth and Atmospheric Sciences and Chemical and Biomolecular Engineering, Georgia Institute of Technology, Atlanta, GA 30332, USA. (thanos.nenes@che.gatech)

G. C. Roberts, Center for Atmospheric Sciences, Scripps Institution of Oceanography, University of California, San Diego, 9500 Gilman Drive, #0239, La Jolla, CA 92093, USA. (greg@fiji.ucsd.edu)